Plasmonic attenuator for infrared imager testing

Robert E. Peale,[a,b,] Pedro N, Figueiredo,[b] Justin R. Phelps,[c] Kevin C. Chan,[c] Reza Abdolvand,[c]

[a]Physics Department, University of Central Florida, Orlando FL 32816, Robert.Peale@ucf.edu; [b]Truventic LLC, 1209 W. Gore St., Orlando FL 32805; [c]Electrical and Computer Engineering, University of Central Florida, Orlando FL 32816

ABSTRACT

We describe a variable attenuator for use with conventional IR quantum cascade or carbon dioxide lasers to create a source with widely and rapidly controllable effective radiant temperature. This would have application to testing of imagers, which must observe scenes that change rapidly between ambient background and very hot objects. The mechanism is controllably frustrated surface plasmon resonance. The device comprises an IR transparent prism with one face coated by a semitransparent (optically-thin) semiconductor having suitable infrared plasma frequency, followed by a controllable gap to a conventional metal mirror. For the mid-wave infrared band (MWIR, 3-5 micron wavelength), we consider a sapphire hemicylindrical prism coated with the transparent conductor gallium-doped ZnO (GZO). For the long-wave infrared band (LWIR, 8-12 micron wavelength), we consider an undoped-Si prism with one heavily-doped surface. Due to the exponential decay of the surface-plasmon-polariton evanescent wave above the conducting film, the log of internal reflectance of the conducting film decreases linearly with increasing gap, typically by about 1 decade per micron, with a total variation of over 5 orders of magnitude. The effective radiance is determined by laser intensity, reflectance, and reflected-beam divergence. Comparison of the effective radiance values to the band radiance of a black body indicates effective radiant temperatures that can be varied from 300 to over 4000 K for a mirror diameter of 100 (MWIR) or 650 (LWIR) microns. At low effective radiant temperature the device can provide 0.1 K resolution.

Keywords: Surface plasmon resonance, infrared, attenuator, conducting oxide, prism

1. INTRODUCTION

An attenuator of IR laser light based on excitation of surface plasmon polaritons (SPP) was recently proposed [1-4]. Theoretical predictions indicate up to 9 orders of magnitude controllable variation in reflected intensity [2]. A potential application is for the calibration of infrared detectors and imagers over a wide range of effective radiant temperature with rapid variation. Effective radiant temperature range and modulation speed would far exceed what can be achieved with conventional black bodies.

Figure 1 schematically presents the attenuator. A key design element is a Kretschmann prism coupler [5] comprising an infrared-transparent prism with one face coated by a partially-transparent (optically thin) conducting film. SPPs are excited by an internally reflected beam on the conducting film. Absorption by the SPP can be frustrated by bringing a metal mirror close to the film, thereby achieving variable attenuation. The metal mirror might be pixelated to create an infrared image based on spatial intensity modulation. Figure 1 suggests one such pixel, with an air gap of dimension *d* that might be controlled with a piezo-electric actuator. After reflection, the beam diverges with solid angle Ω due to the finite aperture of the mirror.

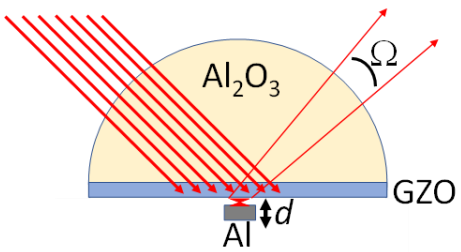

Figure 1. Schematic of plasmonic mid-wave infrared attenuator

The Kretschmann coupler is also the basis of commercial Surface Plasmon Resonance (SPR) biosensors, which operate at visible and near-IR wavelengths [6]. Possible advantages of operating such sensors at mid-and long-wave IR wavelengths, and design considerations, were discussed at least as early as 2008 [7,8]. Those reports emphasized the need for novel conducting films having plasma wavelengths near the IR operating wavelength.

Plasma wavelength may be defined as that where the real part of the permittivity passes through zero and changes sign.The variable IR-attenuator application is better served by an angularly-broad absorption resonance [1-3]. This is achieved when the conducting film has plasma wavelength shorter than, but near, the wavelength to be attenuated. To achieve the highest dynamic range requires the deepest possible absorption, for which the film thickness must be optimized.

Suitable materials with IR plasma wavelengths include conducting oxides and heavily-doped semiconductors [9]. One conducting oxide that has been well studied for plamonics is Ga:ZnO_2 (Gallium-doped Zinc Oxide, or GZO) [10]. In [2], a GZO film on sapphire prism was demonstrated with a metal mirror pressed close to the GZO film to frustrate the MWIR absorption, which qualitatively demonstrated the principle of controllable attenuation.

2. THEORETICAL METHODS

A Kretschmann prism coupler comprises a semi-transparent (optically thin) conducting film on one surface of a transparent dielectric prism [5]. SPPs are resonantly excited when a p-polarized beam is internally incident on the film at a resonance incidence angle beyond the critical angle for total internal reflection within the prism. The resonance angle and absorption depend on wavelength, prism index, film permittivity, and film thickness. Excitation of SPPs decreases the internal specular reflectance of the beam. The resonance-angle condition for exciting SPPs is

$$n \sin \theta_{SPP} = Re \sqrt{\frac{\varepsilon(\omega)}{\varepsilon(\omega)+1}} \quad , \qquad (1)$$

where $\varepsilon = \varepsilon' + i\,\varepsilon''$ is the complex frequency-dependent permittivity of the conducting film, n the prism's refractive index, and θ_{SPP} the resonance angle of incidence within the prism. Eq. (1) resembles the condition for total internal reflection (TIR), namely $n \sin \theta_{TIR} = 1$.

For ordinary metals at IR wavelengths, ε' is negative with magnitude much larger than ε'', so that $\theta_{SPP} > \theta_{TIR}$. However, if $|\varepsilon'|$ is very large, the two angles are almost equal, and the resonance is angularly narrow, which complicates alignment and collimation for optimum attenuation. Broad angular resonances occur when θ_{SPP} significantly exceeds θ_{TIR}, which requires the smaller negative ε' values that occur when the operating wavelength λ is just beyond the conductor's plasma wavelength λ_p.

Resonance strength and angular line shape are accurately calculated using Fresnel's formulae for a multi-layer system. The reflectance of a three-layer system is derived in [11], which is convenient for calculating the reflectivity at the end points $d = \infty$ or 0. The first semi-infinite layer is the transparent prism with real n. The second layer is the conducting film of thickness t and complex permittivity. The third layer is air with real index = 1 or a good metal with complex permittivity. For intermediate d values, we used a 4-layer calculation based on matrix methods [12]. Then the third layer is the air gap of variable thickness d, and the fourth layer is the metal mirror. All calculations were done in MATLAB®.

3. EXPERIMENTAL DETAILS

The GZO film was deposited on the prism coupler by co-sputtering from GaO and ZnO targets in an AJA sputtering system (500 W at 13.56 MHz). The deposition pressure was fixed at 2.55 mTorr. Sputtering was done in pure 20 sccm Ar flow. The power on the ZnO target was 275 W, the prism temperature was 275 ºC. The power on the gallium oxide target was 75 W. Deposition time was 7 minutes and 40 seconds. The Cu prism chuck rested on the heated platen of the sputtering system to heat the prism surface via conduction. Film thickness was measured at a step edge using a Dektak 150 step profilometer on a witness substrate next to the prism. The actual thickness on the prism is expected to exceed that on the witness sample. The sheet resistance of the GZO film on the prism was measured using a 4-point probe.

A quantum cascade laser (QCL) with 4.45 μm center wavelength was used to excite IR SPPs. The laser was polarized with electric field in the plane of incidence (p-polarized) as confirmed using a wire-grid polarizer on BaF_2 substrate. The laser was electrically chopped at 11 Hz by gating the laser driver. Specular reflectance was measured using a motorized goniometer and a pyroelectric detector. The QCL was co-linear with a HeNe laser for alignment purposes, and the reflection of the alignment laser off the front (coated) surface of the prism onto the exit aperture of that laser defined an incidence angle of 180 degrees. The signal from the detector was synchronously amplified by a Stanford SR530 lock-in amplifier, whose output was recorded using Labview.

4. RESULTS

The witness GZO film was 189 nm thick and its resistivity was 0.43 mΩ-cm. Figure 2 (left) presents the measured resonance (black curve) together with the calculation (blue curve). The latter needed to assume a GZO thickness that was 10% higher than indicated by the witness samples, which is roughly the expected tooling factor. The permittivity used to obtain the calculated curve was ε_{GZO} = -13.8+11.1i, which is in reasonable agreement with permittivity measured by ellipsometry for similar GZO films [4,10]. For Al at 4.45 μm wavelength the permittivity value ε_{Al} = -2580 + i 780 was determined from the Drude parameters [13]. The prism index was taken to have the value [14] n_{Al2O3} = 1.652. The agreement between experiment and calculation is very good in the region of the resonance, which gives us confidence in the calculations used to optimize the GZO thickness and in the resulting values of resonance angle and minimum reflectance.

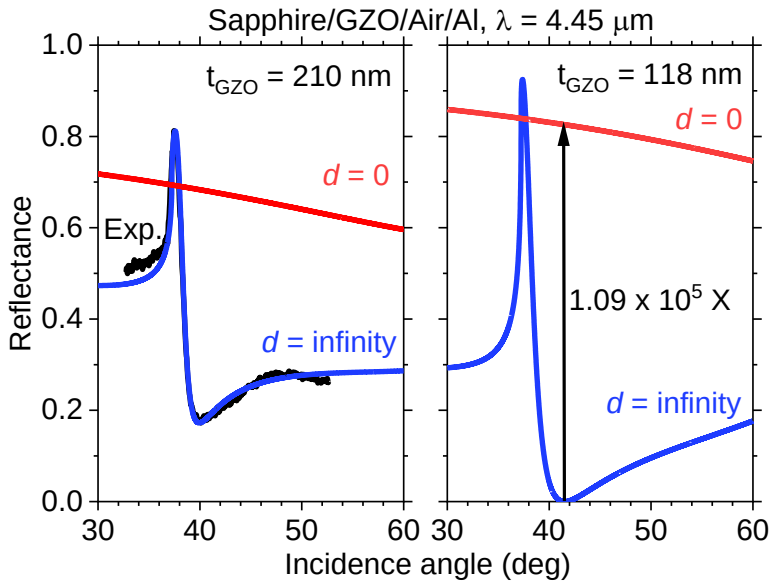

Figure 2. (left) Experimental MWIR reflectance vs incidence angle together with calculated curves for the indicated air gaps. (right) Calculated curves for optimized GZO thickness.

The optimization of t_{GZO} stepped this value in 1 nm units. A deeper theoretical resonance can be achieved by using smaller steps [2], but 1 nm already pushes the fabrication tolerances. Figure 1 (right) presents the calculated curves for the optimized GZO thickness of 118 nm. The minimum reflectance occurs when *d* is large at an incidence angle of 41.5 deg, where R = 7.6 x 10^{-6}.

The red curves with slow monotonic decrease in Figure 2 were calculated by replacing air with Al as the third layer. For this *d* = 0 situation and optimized t_{GZO}, R = 0.83 at the resonance angle. The ratio, indicated in Figure 2 (right), exceeds five orders of magnitude. The values of the red curve in Figure 2 (left) are lower than in Figure 2 (right) because the beam must transit more of the lossy GZO before being reflected by the Al. For the same reason, these red curves monotonically decrease with increasing incidence angle.

Controllable attenuation is achieved by varying the air thickness continuously between 0 and infinity. This calculation requires the 4-layer code. The 3- and 4-layer codes were developed and executed independently by the two lead authors as a check on the results. Figure 3 (left) compares the results for the optimized conditions of Figure 2 (right). We see that the results at and beyond the SPP resonance are indistinguishable for the two calculations. Besides confirming the different codes, we see that for the SPP resonance a gap of 10 μm is already equivalent to one of infinity. Below the θ_{TIR} angle, however, the curves differ markedly due to Salisbury-screen resonances [15] in the air-gap for finite *d*. The peaks occur when the wave in the gap has a node at the lossy GZO.

Figure 3 (right) presents calculated reflectance as a function of air-gap *d* between GZO surface and Al mirror for the optimized device. The incidence angle is that for which R is minimum at large *d*. The reflected intensity is a minimum for large gaps. The exponential variation exceeds one decade per micron with a range of more than 5 orders. The variation is slow at large gaps. Between d = 9 and 10 μm, R varies by only 10^{-8}. Between 10 μm and infinity, the variation is only twice this.

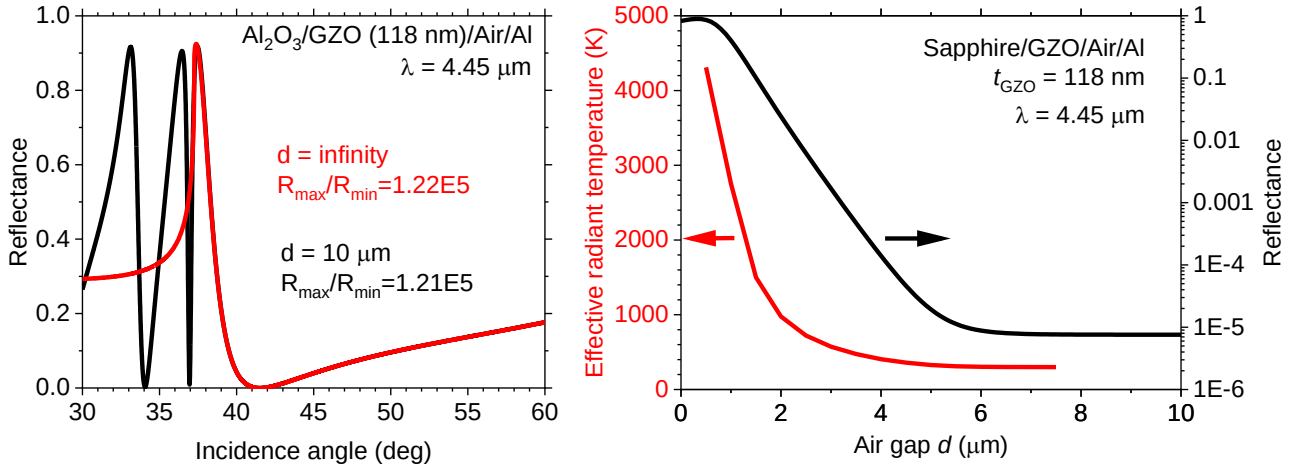

Figure 3. (left) Comparison of 3- and 4-layer calculations for large air gap. (right) Reflectance and effective radiant temperature of optimized device as a function of air gap.

The dynamic range of an IR detection system is often defined in terms of the temperature of a blackbody source. The effective radiant temperature of a non-blackbody source is the temperature of a blackbody that gives the same spectral radiance as the source [16]. The curve of blackbody temperature vs radiance within a given wavelength band is calculated from the Planck function. Radiation within the given band that is reflected with a certain power per unit mirror area and with a certain divergence solid angle has an effective radiance, which may be compared with the band radiance of a blackbody to define an effective radiant temperature for the mirror. If a monochromatic plane wave with wavelength in the given band and intensity I is reflected from a mirror with aperture p and reflectance R, as suggested in Figure 1, the reflected beam diverges with solid angle $\Omega = (\lambda/p)^2$, and the radiance is $I\,R\,/\,\Omega$.

To give a concrete numerical example, suppose I = 50 mW/cm^2, λ = 4.45 μm, and p = 100 μm. Then Ω = 0.0020 sr, which would fill a 5 cm entrance aperture for an imaging system at a distance of 1 meter. The wavelength is within the MWIR band, which we suppose is the detection range for the system under test. For the reflectance limits of Figure 2 (right), namely 7.6 x 10^{-6} to 0.83, the radiance would range from 1.87 to 203000 W/m^2-sr. These values for the MWIR band correspond to blackbody temperatures of 300 and 4200 K, respectively. That range of effective radiant temperatures extends from room temperature up to the combustion temperature in a rocket engine. Such a range would be a challenge for conventional blackbody sources.

Figure 3 (right) presents a plot of effective radiant temperature vs. air gap for the considered example. A promising feature demonstrated by this curve is that the change in low effective radiant temperatures with gap is very slow. Effective radiant temperature rises with decreasing gap by only 1 K/μm between gaps d = 6.5 and 7.5 μm. One could control the gap to within 100 nm using commercial piezoelectric actuators (e.g. ThorLabs PIAK10), giving a temperature resolution of 0.1 K, which is about what is required near ambient temperature for IR imagers. Moreover, effective radiant temperature changes widely with tiny movements of a mirror, so it could be altered much more rapidly than the actual temperature of a conventional blackbody.

Sapphire or CaF_2 prisms are useful for MWIR wavelengths, but they have no or low transmittance in the LWIR. A ZnSe prism might be used, but its cost, and the complexity of depositing a suitable film with LWIR plasma frequency on it motivate a different solution, namely silicon plasmonics [9]. The complex permittivity of silicon may be tailored by doping. We have experimentally demonstrated the excitation of LWIR SPPs on heavily-doped silicon [9]. Permittivity of p-type Si with dopant concentration 10^{20} cm^{-3} is ε = -16.19 +i 20.96 at the CO_2 laser wavelength 10.59 μm [9]. As SPP host, we suppose an ion-implanted layer with that concentration to a depth of 244 nm on the active surface of an undoped Si-prism. We take n_{Si} = 3.42, for which θ_{TIR} = 17 deg. At 10.59 μm wavelength [13], ε_{Al} = -10668 + 7457i. Figure 4 (left) presents the SPP-resonance calculation. The minimum reflectance R_{min} = 4.49 x 10^{-6} occurs at 18.3 deg, and R = 0.752 for d = 0. The ratio = 1.7 x 10^5. The R vs d and effective radiant temperature curves are presented in Figure 4 (right). Note that while the distance over which R varies from max to min is about 15 μm, while the distance over which effective radiant temperature varies over the likely useful range is only half this value. Thus, tolerances may be relaxed, and a dynamic range in R of 1000 may suffice.

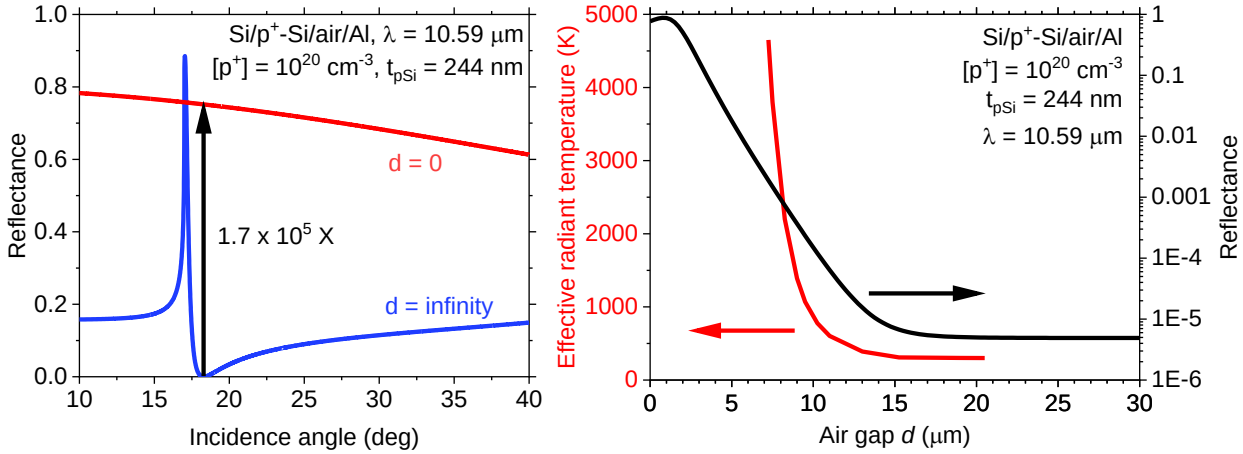

Figure 4. (left) Calculated LWIR resonance for Si prism. (right) Reflectance and effective radiant temperature of optimized Si plasmonic LWIR attenuator as a function of air gap.

4. DISCUSSION AND SUMMARY

In summary, this paper presented predictions for an infrared plasmonic laser attenuator based on controllably-frustrated surface-plasmon-resonance using a Kretschmann coupler. A range of effective radiant temperatures from 300 K to over 4000 K are considered achievable in both MW- and LWIR bands using suitable materials. The effective radiant temperature might be varied or modulated at high speed using commercial actuators. Such performance greatly exceeds the possibilities of conventional black-body sources.

ACKNOWLEDGMENTS AND DISCLOSURE

Work by Truventic authors was internally funded. UCF authors acknowledge partial supported by the Florida High Tech Corridor Council. REP and PNF have a financial interest in Truventic, and these authors may profit from the results of this research.

REFERENCES

1. Figueiredo, P., Peale, R., "Plasmonic infrared attenuator," Proc. IEEE RAPID (Research and Applications of Photonics in Defense) Aug 19-21, 2019, Miramar Beach FL, paper number TuA1.3, DOI: 10.1109/RAPID.2019.8864416
2. Figueiredo, P. N., DeMonaco, S. R., Phelps, J. R., Abdolvand, R., Peale, R. E., "Plasmonic infrared-laser attenuator," Infrared Physics & Technology 111, 103561 (2020).
3. Figueiredo, P. N., "Scene generation using surface plasmon polaritons," US Patent No. 10,788,360, Sep. 29, 2020.
4. Peale, R. E., Figueiredo, P. N., Phelps, J. R., Chan, K. C., Abdolvand, R, Smith, E. M., Vangala, Shivashankar, "Infrared surface-plasmon-resonance attenuator for broadly controllable effective radiant temperature," Infrared Physics and Technology, accepted (2022).
5. Kretschmann, E., Die Bestimmung optischer Konstanten von Metallen durch Anregung von Oberflächen-plasmaschwingungen, Z. Phys. 241, 313 (1971).
6. Homola, J., Yee, S. S. and Gauglitz, G. "Surface Plasmon Resonance Sensors: Review," Sens. Actuators B Chem. 54, 3 (1999).
7. Cleary, J. W., Peale, R. E., Shelton, D., Boreman, G., Soref, R., and Buchwald, R. W., "Silicides for infrared surface plasmon resonance biosensors," MRS Online Proceedings Library **1133**, Article number 1003 (2008).
8. Cleary, J. W., Medhi, G., Peale, R. E., Buchwald, W. R., Edwards, O. and Oladeji, I., "Infrared Surface Plasmon Resonance Biosensor," Proc. SPIE **7673**, 767306 (2010).
9. Shahzad, M., Medhi, G., Peale, R. E., Buchwald, W. R., Cleary, J. W., Soref, R., Boreman, G. D., and Edwards, O., "Infrared surface plasmons on heavily doped silicon," J. Appl. Phys. 110, 123105 (2011).
10. Gibson, R., Vangala, S., Oladeji, I. O., Smith, E., Khalilzadeh-Rezaie, F., Leedy, K., Peale, R. E., and Cleary, J. W., "Conformal spray-deposited fluorine-doped tin oxide for mid- and long-wave infrared plasmonics," Optical Materials Express **7**, 2477 (2017).
11. Landau, L. D., Lifshitz, E. M., and Pitaevskii, L. P., Electrodynamics of Continuous Media, 2nd Edition, Section 86, Problem 4.
12. Hecht, E. and Zajac, A., Optics (Addison-Wesley, 1974), section 9.9.1.
13. Ordal, M. A., Bell, R. J., Alexander, Jr., R. W., Long, L. L., and Querry, M. R., "Optical properties of fourteen metals in the infrared and far infrared: Al, Co, Cu, Au, Fe, Pb, Mo, Ni, Pd, Pt, Ag, Ti, V, and W," Appl. Opt. 24, 4493 (1985).
14. Palik, E. D., Handbook of Optical Constants of Solids II (Academic, 1991), Chapter "Aluminum Oxide (Al_20_3)" by Gervais, F., p. 761.
15. Salisbury, W. W., "Absorbent Body for Electromagnetic Waves," U.S. patent 2,599,944 (1952).
16. Hudson, Jr., Richard D., Infrared System Engineering (Wiley Interscience, 1969).